



ORIGINAL ARTICLE

Surface structure–activity relationships of Cu/ZnGaO_x catalysts in low temperature water–gas shift (WGS) reaction for production of hydrogen fuel

Venkata D.B.C. Dasireddy^{a,b,*}, Karmina Rubin^a, Andrej Pohar^a, Blaž Likozar^a

^a Department of Catalysis and Chemical Reaction Engineering, National Institute of Chemistry, Hajdrihova 19, 1001 Ljubljana, Slovenia

^b Faculty of Engineering and Built Environment, The University of Newcastle, 2308 Callaghan, Australia

Received 26 December 2019; accepted 10 February 2020

Available online 26 February 2020

KEYWORDS

Syngas;
Hydrogen;
Cu/ZnGaO_x catalyst;
Water–gas shift (WGS);
Steam reforming reactions;
Fuel cell systems

Abstract A new species' class of Cu-, Ga- and Zn-based rate catalysts was prepared by a systematic co-precipitation technique at the different related pH values (6.5–8.0) along with calcination functional conditions, influencing components' physical properties, these were characterized, and their application performance for water–gas shift (WGS) reaction was researched. Substances were analysed by various experimental methods, namely chemisorption, temperature-programmed reduction (TPR) characterisation, diffraction, physisorption and microscopy. A homogenous size dispersion of the compounds with smaller granular particles was obtained for catalysis, implemented with high pH-resulting outputs. H₂ TPR profiles revealed a tailored stronger effect of Cu–Zn on Ga for process, operated with low pH-conditioned forms. Over Cu/ZnGaO_x, WGS was sensitive to Cu, which was primarily active. Catalytic chemical reactivity, activity and selectivity were also found to be critically dependent on material lattice structure, copper surface area and metal–support interaction phenomena. The temperature-programmed surface reaction with mass spectrometry (TPSR–MS) measurements showed that formulations, synthesised at the pH of 8.0, enabled reaching >99% of the equilibrium yield CO conversion at 260 °C. An increase in the converted CO, oxidation and H₂ productivity with the integral steam content in gaseous feed flow was achieved. The heterogeneous phase processing at the correlated pH of 7.6 demonstrated the highest formed CO product at the temperature of 200 °C, compared with literature. This is particularly

* Corresponding author at: Department of Catalysis and Chemical Reaction Engineering, National Institute of Chemistry, Hajdrihova 19, 1001 Ljubljana, Slovenia.

E-mail addresses: dasireddy@ki.si, venkata.dasireddy@newcastle.edu.au (V.D.B.C. Dasireddy).

Peer review under responsibility of King Saud University.



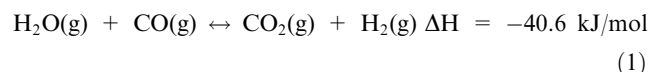
Production and hosting by Elsevier

promising for reagent purity hydrogen-fed fuel cells. The kinetics for each co-precipitated solid was evaluated regarding the efficiency for the WGS in a fixed bed reactor.

© 2020 Published by Elsevier B.V. on behalf of King Saud University. This is an open access article under the CC BY-NC-ND license (<http://creativecommons.org/licenses/by-nc-nd/4.0/>).

1. Introduction

Felice Fontana discovered the WGS reaction in 1780, and it is traditionally used for the production of hydrogen (Reitz, 2007). It was first reported in 1888 (Mond, 1889), and in 1913 (Carl, 1914) the reaction was applied industrially in the Haber ammonia synthesis process, while Bosch and Wilde developed the catalyst (Twigg, 1996). Furthermore, the WGS reaction has a significant impact on the hydrogen fuel process, Fischer-Tropsch reaction, ammonia and methanol syntheses, steam reforming of methane and methanol, etc. (Smith et al., 2010). The WGS reaction is a catalytic–reversible–chemical reaction, whereby CO₂ and H₂ are produced by the reaction of CO and steam (Eq. (1)):



WGS reaction is thermodynamically favourable at lower temperatures due to exothermic properties, corresponding to lower reaction rates; on the other hand, higher temperatures indicate higher reaction rates (Gokhale et al., 2008). Catalysts for the WGS reaction are a variety of metals and metal oxides such as Fe (Boudjemaa et al., 2009), Cu (Si et al., 2012), Au (Aejjels Averink Silberova et al., 2006), Ru (Basińska et al., 1999), and Pt (Chenu et al., 2005). For commercial purposes the WGS reaction is performed in two distinct stages: LT–WGS (low-temperature WGS reaction) at temperatures 150–250 °C, and HT–WGS (high-temperature WGS reaction) at temperatures 350–450 °C. Catalysts based on Fe are used for HT–WGS reaction, while Cu-based catalysts are known for LT–WGS reaction (Ratnasamy and Wagner, 2009); and a broad-temperature shift over molybdenum oxide-promoted (CoMo-based) catalysts (Mi et al., 2017). According to the literature (Chenu et al., 2005), some efforts have been devoted to developing the low-temperature activity of CoMo WGS catalyst. Metals such as Zr, Ti, Pt, Ru, and Au were added to CoMo-based catalysts result in high WGS activities at low-temperature (Chenu et al., 2005; Mi et al., 2017). Cu-based catalysts are widely used, because of their cost-effectiveness, high catalytic behaviour, and selectivity as compared to other metals (Thinon et al., 2008). Studies have shown high WGS activity for Cu/CeO₂ catalyst (Si et al., 2012) and it was observed that the incorporation of Cu/ZnO with another oxide support (Al₂O₃; MgO or CeO₂) correspond to high WGS activity when compared to Cu catalysts supported on SiO₂/Al₂O₃, SiO₂/MgO or zeolite support (Yahiro et al., 2007). In general, the metal and the support have an important role in the catalyst properties and performance (Panagiotopoulou et al., 2006).

Recently, researchers on direct methanol steam reforming for the production of H₂ over CuZnGaO_x catalysts (Aejjels Averink Silberova et al., 2006; Toyir, 2015) and a study on the *beta*-brass catalyst of Cu–Zn doped with Ga³⁺ for the generation of ethylene glycol (Li et al., 2016) showed high catalytic performance. Adding selected precursors to Cu-based catalysts

can be rationalised with ionic radii of elements, while they are nearby to each other in the periodic system (Cu²⁺ = 8.7 pm, Zn²⁺ = 8.8 pm, Ga³⁺ = 7.6 pm). Therefore, Ga and Zn incorporation into a Cu-based catalyst structure would lead to crystal defects, due to swapping and substitution among these ions that could correspond to suspended crystal growth. The incorporation of Ga³⁺ into a Cu-based catalyst plays a significant role in the catalyst structure due to the increase in the dispersion of Cu (Tong et al., 2013).

Catalyst preparation consists of many important parameters: pH, temperature, mixing, aging, etc., which has a crucial impact on catalyst morphology. Structure, surface area and metal dispersion of catalysts are dependent on pH (Schüth and Unger, 2008). Experiments for Cu/Zn/Al catalysts, obtained with the titration method, have shown that when pH slowly increases, Cu is precipitated first (Behrens and Schlögl, 2013). For precipitation of Cu–Zn at different pH values (4–10) and temperatures (30–70 °C), differences in the Cu⁰ surface areas after reduction at 300 °C were observed. The surface area decreased with a decrease in pH value during precipitation, where for the lowest surface area, large CuO crystallites were observed (Baltes et al., 2008). This is in agreement with previous researchers (Behrens and Schlögl, 2013; Baltes et al., 2008) which shows higher Cu⁰ surface areas at a pH of 6–7. In our previous work (Rubin et al., 2018), it has been shown that the catalyst prepared at a pH of 7.4 showed a high activity in the water gas shift catalyst.

In the present work, Cu-based catalysts were prepared by the co-precipitation method at different constant pH values (6.5–8.0). The influence of co-precipitation parameters on the catalyst structure and its performance were tested for the LT–WGS reaction in a packed bed reactor. Physical properties of CuZnGaO_x catalysts were characterized by various methods such as Brunauer–Emmett–Teller (BET) surface analysis, powder X-ray Diffraction (XRD), Scanning Electron Microscopy (SEM) coupled with Energy-Dispersive X-ray spectroscopy (EDS), Temperature Programmed Reduction with H₂ (H₂-TPR), Temperature Programmed Desorption (CO, H₂ and CO₂) and N₂O chemisorption.

2. Experimental

2.1. Catalyst preparation

CuZnGaO_x catalysts with the molar ratio Cu: Zn: Ga = 5: 3: 2 (48.7: 31.3: 20 precisely) were synthesised by the co-precipitation method at different constant pH values, i.e. 6.5, 6.9, 7.6, and 8.0. All nitrate metal salts (Aldrich) were mixed in 100 mL of distilled water, and Na₂CO₃ (Aldrich) was also dissolved in the same amount of distilled water. Solutions were dispensed to a 500 mL Erlenmeyer flask filled with 300 mL distilled water, which was preheated to 80 °C. Flow rates of nitrate solution and sodium solutions at the start of co-precipitation were identical (0.1, 0.5, 1 and 2 mL/min). The

pH was controlled with pH electrode (Metrohm) and maintained at constant pH with a variation of the flow rate of Na₂CO₃ solution. The resulting co-precipitate was aged at the same temperature for about 4 h. After aging, it was washed with distilled H₂O, for Na⁺ ions elimination, and was separated from the solution with laboratory vacuum filtration. Then the precipitate was dried for 24 h at 95 °C in N₂ with the flow rate 50 mL/min, excluding catalyst CZG(8.0) which was dried for 12 h at the same conditions. After drying the calcination step followed. The co-precipitate was calcined in an oven from room temperature to 90 °C and maintained for 30 min. Afterward, it was heated to 300 °C for 2 h and maintained at that temperature for 4 h, excluding catalyst CZG(6.9)-2h which was maintained at that temperature for only 2 h. Catalysts were named according to the co-precipitated pH value.

2.2. Catalyst characterization

All co-precipitated catalysts were characterised with N₂ physisorption, where the BET specific surface areas were measured with Micromeritics ASAP 2020. Powder X-ray diffraction (XRD) data for a catalyst was analysed on a PANalytical X'Pert PRO MPD at room temperature. With the Scherrer equation, the crystallite size was calculated, and with the Williamson–Hall (W–H) analysis the lattice strain was evaluated (Mote et al., 2012; Khorsand Zak et al., 2011; Jha et al., 2016). With the chemisorption analyser Micromeritics AutoChem II the Temperature Programmed Reduction with Hydrogen (H₂-TPR) and Temperature Programmed Desorption (CO, H₂, and CO₂) analyses were obtained. The metal dispersion was measured by using dissociative N₂O chemisorption according to the procedure explained in the literature (Yuan et al., 2011; Luo et al., 2012). Scanning Electron Microscopy (SEM) and Energy Dispersive Spectroscopy (EDS) analyses were obtained with the electronic microscope FE–SEM SUPRA 35–F (Carl Zeiss) equipped with the dispersive energy spectrometer Inca 400 (Oxford Instruments). The Temperature Programmed Surface Reaction–Mass Spectroscopy (TPSR–MS) measurements were obtained with Micromeritics AutoChem II analyser incorporation with a ThermoStar TM GSD 301T (Pfeiffer Vacuum) mass spectrometer. Procedures of mentioned analysis are described in the [supplementary information Electronic supplement information, Section 1 Catalyst characterization](#).

2.3. Catalytic testing

Approximately 1 g of calcined catalyst was placed into a packed bed tubular reactor and stabilised with glass wool on both sides. The tubular reactor was installed into the hot box of the PID Microactivity-Reference Reactor (Process Integral Development S. L., Spain), equipped with a Gilson 307 HPLC Pump for feeding liquid samples; in these study, it was distillate water. A 490 Micro GC (Agilent Technologies, Santa Clara, USA) with two columns (20 m MS5Å and 10 m PPU) with 8.5% H₂/He as the reference flow were connected to the outlet of the system. Water was condensed at the exit of the reactor, while the permanent gases (CO, CO₂, H₂, N₂, O₂, and CH₄) were analysed. Furthermore, each catalyst was activated by reduction with pure hydrogen (99.999%,

Messer). The activation of the catalyst was carried out with H₂ at the flow of 7.5 mL/min through the reactor from room temperature to 300 °C and maintained at that temperature for 2 h. After activation catalyst was purged with pure N₂ at the flow rate of around 50 mL/min until the temperature decreased to room temperature. Catalysts were purged with N₂ overnight or several hours prior to each measurement to remove any adsorbed reactants or products. The evaluation of a catalyst followed by an analysis of different temperatures, flow rates and molar ratios of H₂O to CO (STCO).

With the obtained measurements, CO conversion was calculated by:

$$CO_{\text{conversion}} (\%) = \frac{[CO_{\text{in}}] - [CO_{\text{out}}]}{[CO_{\text{in}}]} \times 100 \quad (2)$$

where $[CO_{\text{in}}]$ represent a CO molar flow rate in the reactor and $[CO_{\text{out}}]$ a CO molar flow rate out of the reactor, both in mL/min. Each measurement was run at least 2 h in a stationary state, for which more than 20 data points were collected with a standard deviation of around 1%.

3. Results and discussion

The particle size and surface area of a catalyst were characterised with BET surface area (S_{BET}) (Table 1). For Cu–Zn based catalysts, surface areas were between 1 and 110 m²/g, depending on catalyst preparation (Shishido et al., 2004; Agrell et al., 2001; Cai et al., 2015). In this study, the surface areas are ranged between 55 and 125 m²/g. S_{BET} has an important influence on the catalytic activity (Hadden et al., 1995). Baltes et al. (2008) reported, due to the research of the impact of different co-precipitation parameters (pH, precipitation and temperature of calcination) on a Cu/ZnO/Al₂O₃ catalysts, higher catalytic behaviour for the synthesis of methanol for catalysts co-precipitated at neutral or even slightly acidic pH. Many authors (Behrens and Schlögl, 2013; Baltes et al., 2008; Behrens, 2009) reported a significant impact of the precipitate pH value on the composition phases in a catalyst. It has been proposed that when pH decreases, H⁺ ions concentration increases, which leads to a decrease in the concentration of carbonate, which then leads to an increase in the copper phase composition in a catalyst. In this study, the highest BET surface area of calcined catalysts corresponds to catalysts CZG(7.6) and CZG(8.0), 124 m²/g, while the catalyst CZG(6.9)-2h showed the lowest surface area, 58 m²/g. Catalysts CZG(8.0) and CZG(6.5) have the highest pore volumes of 0.33 m³/g, while CZG(6.9)-2h has the lowest, 0.15 m³/g. The S_{BET} for calcined catalyst CZG(8.0) was lower for 31 m²/g compared to uncalcined CZG(8.0)-UN; also pore volume and size were lower for calcined catalyst CZG(8.0). A decrease in S_{BET} for calcined catalysts compared with uncalcined catalysts corresponds to a change in a catalyst structure, which was also obtained in the literature (Hodge et al., 2002). For uncalcined catalyst, CZG(8.0)-UN higher crystalline peaks are obtained with the XRD profile compared to calcined catalyst CZG(8.0). A significant impact of a calcination, calcination temperature, on a catalytic activity and catalyst surface area has been reported: calcined catalysts have lower surface area than uncalcined catalyst; surface area decreases with an increase in temperature of calcination, because of enlarging and sintering in size of particle at higher temperature; and surface area of used catalyst was lower than

Table 1 Properties of CuZnGaO_x catalyst co-precipitated at different pH values.

| Catalyst | Composition Cu/Zn/Ga [%] | S_{BET}^c [m ² /g] | Pore volume ^c [m ³ /g] | D_{Cu}^d [%] | S_{Cu}^d [m ² _{Cu} /g _{Cu}] | Average crystallite size (nm) ^e |
|------------------------------|-----------------------------|---|---|--------------------------|--|--|
| CZG(6.5) | 48.5/32.3/19.2 | 109 | 0.33 | 27 | 186 | 19 |
| CZG(6.9)-2h ^a | 47.3/32.0/20.7 | 58 | 0.15 | 51 | 344 | 22 |
| CZG(6.9) | 43.8/32.1/24.1 | 88 | 0.19 | 74 | 502 | 33 |
| CZG(7.6) | 50.1/31.3/18.6 | 124 | 0.32 | 28 | 189 | 12 |
| CZG(8.0) | 51.1/30.2/18.8 | 124 | 0.33 | 27 | 185 | 12 |
| CZG(7.6)- UN ^b | 51.1/30.3/18.6 | 146 | 0.64 | / | / | 33 |
| CZG(8.0)- UN ^b | 50.3/29.6/20.1 | 155 | 0.67 | / | / | 44 |

^a Calcined for 2 h.

^b Uncalcined catalyst.

^c N₂ physisorption.

^d N₂O chemisorption.

^e Calculated using Scherrer equation and XRD profile.

of un-used catalyst attributed to deposition of carbon (Al-Fatesh and Fakeeha, 2012; Li et al., 2016). After WGS measurements of co-precipitated catalyst CZG(7.6) showed a decrease in surface area from 124 to 83 m²/g. The surface area decrease for once calcined catalyst CZG(6.9)-2h from 58 to 56 m²/g and for the twice calcined catalyst CZG(6.9) from 88 to 31 m²/g. This can be due to the carbon deposition on a surface of the catalyst during WGS reaction which is also identified by Raman spectroscopy (not shown).

From SEM images it can be observed that all catalysts showed defined structured clusters of particles with a change in morphology in order with pH values of catalyst preparation (Fig. 1). Catalysts CZG(6.5), CZG(7.6) and CZG(8.0) show a relatively alike morphology with smaller particles in comparison with catalysts prepared at other pH values i.e. CZG(6.9)-2h and CZG(6.9). Calcined catalyst CZG(7.6) showed a high crystalline nature of the particles compared to uncalcined catalyst CZG(7.6)-UN, which suggests that calcination increases the crystalline nature of catalysts (Electronic supplementary information Fig. S1). Research (Faungnawakij et al., 2007) has shown the influence of calcination temperature on the reducibility and crystallinity of CuFe₂O₄ (spinel of copper ferrite) and also on alumina acidity. The importance of calcination temperature and catalyst structure indicated an increase in crystallinity and crystallite size with an increase of calcination temperature. EDS elemental composition of catalysts, in this study, is in agreement with nominal metal loading in catalysts.

The catalyst synthesised at pH value at 6.5 corresponds to the highest approach to the theoretical composition of Cu/Zn/Ga, while the catalyst prepared at pH value at 8.0 has shown the lowest approach (Table 1). The increase in the content of the copper phase in a catalyst is depended on the formation of malachite and other hydroxy carbonates, which is conditional on the pH value of preparation. With an agreement in the literature (Baltes et al., 2008) the amount of copper present in the catalyst increases with an increase in pH. The highest atomic % value of Cu corresponds to calcined catalyst CZG(8.0) (51.1%), while the lowest to the once calcined catalyst CZG(6.9)-2h (47.3%) and twice calcined catalyst CZG(6.9) (43.8%). Researches (Behrens and Schlögl, 2013; Behrens, 2009) have shown that catalysts prepared at acidic pH

suppressed malachite formation and other hydroxy carbonates, which leads to the increase in copper phase content in the catalysts, which is in agreement with this study (Electronic supplementary information Fig. S2). A comparison between uncalcined and calcined catalyst co-precipitated at pH value 7.6 showed lower atomic % of Cu and Zn for the calcined catalyst, CZG(7.6), while for catalyst synthesised at pH value 8.0, in comparison uncalcined to calcined, is lower for the uncalcined catalyst, CZG(8.0)-UN. The value of the atomic % of Ga did not change for the uncalcined and calcined catalyst prepared at pH value 7.6, 18.6%. On the other hand, atomic % of Ga for catalyst co-precipitated at pH value 8.0 decreases after calcination from 20.1% to 18.8% (Table 1). Lower values of atomic % of Cu and Zn for calcined catalysts CZG(7.6) and CZG(8.0) compared to uncalcined catalysts, CZG(7.6)-UN and CZG(8.0)-UN, indicate the importance of calcination.

Furthermore, the main diffraction peak for all calcined CuZnGaO_x catalysts in XRD pattern (Fig. 2(a)) are well distinguished at 2θ values of 35.6° (111) with a d-spacing of 2.52 Å, also at a 2θ values of 38.8° (1 1 1) and 48.1° (202) with a d-spacing of 2.32 Å and 1.89 Å can be attributed to CuO (JCPDS 05-0661) (Tong et al., 2013). CuO diffraction peaks in XRD patterns show high intensity for catalysts CZG(6.9) and CZG(6–9)-2h, and low intensity for catalyst CZG(8.0), which is in agreement with the copper content in the catalysts. CuO peak (1 1 1) is clearly visible for catalyst CZG(6.9)-2h, CZG(6.9) and CZG(6.5), while for catalysts CZG(7.6) and CZG(8.0) this peaks is observed as an amorphous shoulder. The peak corresponding to CuO (111) is broader for catalysts CZG(7.6) and CZG(8.0) as compared with other catalysts, which is a result of the amorphous nature obtained by preparation at basic pH, while for all other catalysts, excluding CZG(6.9)-2h, where this peak is low and a bit broader, that peak is more narrow and intense, which can be attributed to particle sintering, a more arranged structure and crystallite growth. For the catalyst CZG(8.0), the peak CuO (202) is not detected. Furthermore, peaks observed at 2θ values of 30.3°, 57.3° and 62.8° with a d-spacing of 2.91 Å, 1.61 Å and 1.48 Å coincide to the cubic spinel ZnGa₂O₄ phase (JCPDS 38-1240) (De souza Gonçalves et al., 2006). Other peaks at values 2θ of 43.3°, 17.4° and 18.1° with a d-spacing of 2.09 Å, 4.94 Å

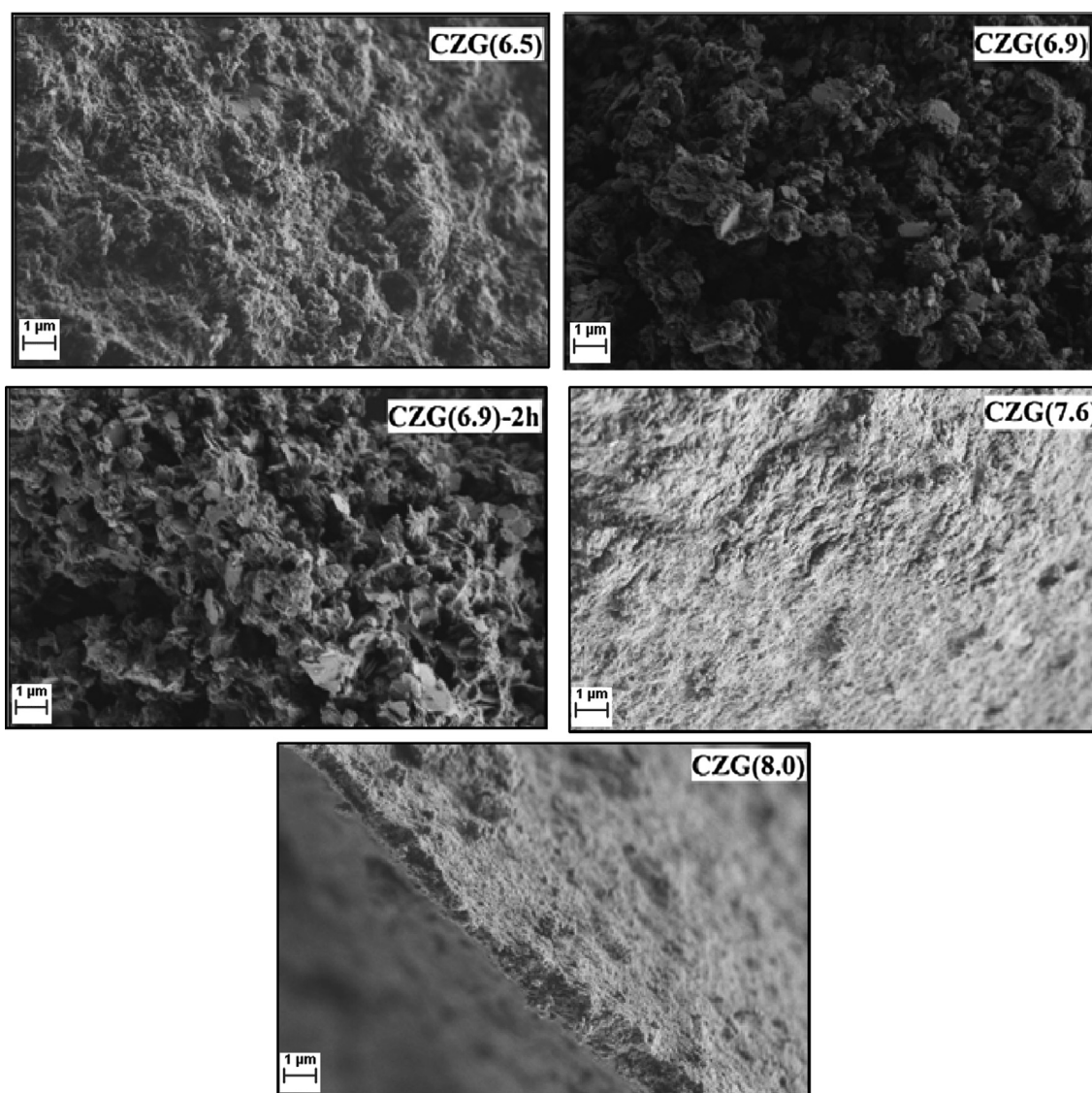


Fig. 1 SEM images of calcined catalysts CZG(6.5), CZG(6.9)-2h, CZG(6.9), CZG(7.6) and CZG(8.0).

and 5.11 \AA also indicates a ZnGa_2O_4 phase, excluding CZG(6.9)-2h. XRD of catalyst CZG(6.9)-2h contains two peaks at a 2θ of 11.6° and 23.3° with a d-spacing of 7.62 \AA and 2.68 \AA indicates that zincian malachite $(\text{CuZn})_2\text{CO}_3(\text{OH})_2$ (JCPDS 36-1475) (Melian-Cabrera et al., 2002) is still present in the structure of the catalyst.

Jung et al. (2010) studied precursor structures during the aging of catalysts $\text{Cu/ZnO/Al}_2\text{O}_3$ and found out that the final structure of precursors was malachite and that aging has also a very important influence on a precursors structure. Bart and Sneeden (1987) have shown that a hydroxyl carbonate phase presence after calcination influence on final catalytic quality of $\text{Cu/ZnO/Al}_2\text{O}_3$ catalysts. During a reduction of $\text{Cu/ZnO/Al}_2\text{O}_3$ catalysts hydroxy carbonates purportedly facilitated a formation of catalytic active sites. Therefore, a constant pH value of catalyst preparation also affected the physical appearance of the catalyst. Colour at the end of co-precipitation for catalysts CZG(6.5), CZG(6.9)-2h, and CZG(6.9) was dark brown, while for catalysts CZG(7.6) and CZG(8.0) was turquoise. It can be concluded on colours of catalysts precursors

at the end of the aging that for dark brown colour more oxides phases were present in the precursor, while for turquoise colour precursor's malachite phase prevailed, which is in correlation with the literature (Su et al., 2015).

Furthermore, there is no presence of Ga_2O_3 phase observed in the CuZnGaO_x catalysts. This can be attributed to a highly disperse amorphous state of Ga_2O_3 which may not be detectable by XRD analysis. It was shown in the literature (Tong et al., 2013; Yu et al., 2012) that $\alpha\text{-Ga}_2\text{O}_3$ phase is not present in CuZnGaO_x catalyst, due to the formation of a poorly crystalline tetragonal spinel CuGa_2O_4 phase. Thus, catalyst CuGaO_x consists of two phases, a tetragonal spinel CuGa_2O_4 , and a surplus CuO phase. With the addition of Cu to catalyst, cubic spinel phase ZnGaO_x was obtained in CuZnGaO_x catalyst, while the ZnO phase was not indicated, due to a well-dispersed excess of Zn^{2+} in the catalyst. Due to ligand field stabilisation energy (LFSE), spinel comprising Cu is an inverse spinel structure, where O_h sites are filled by Cu^{2+} (d9 configuration), T_d sites by Ga^{3+} (d10) and Zn^{2+} (d10) occupied whether in T_d or O_h sites. Nevertheless, in the spinel structure

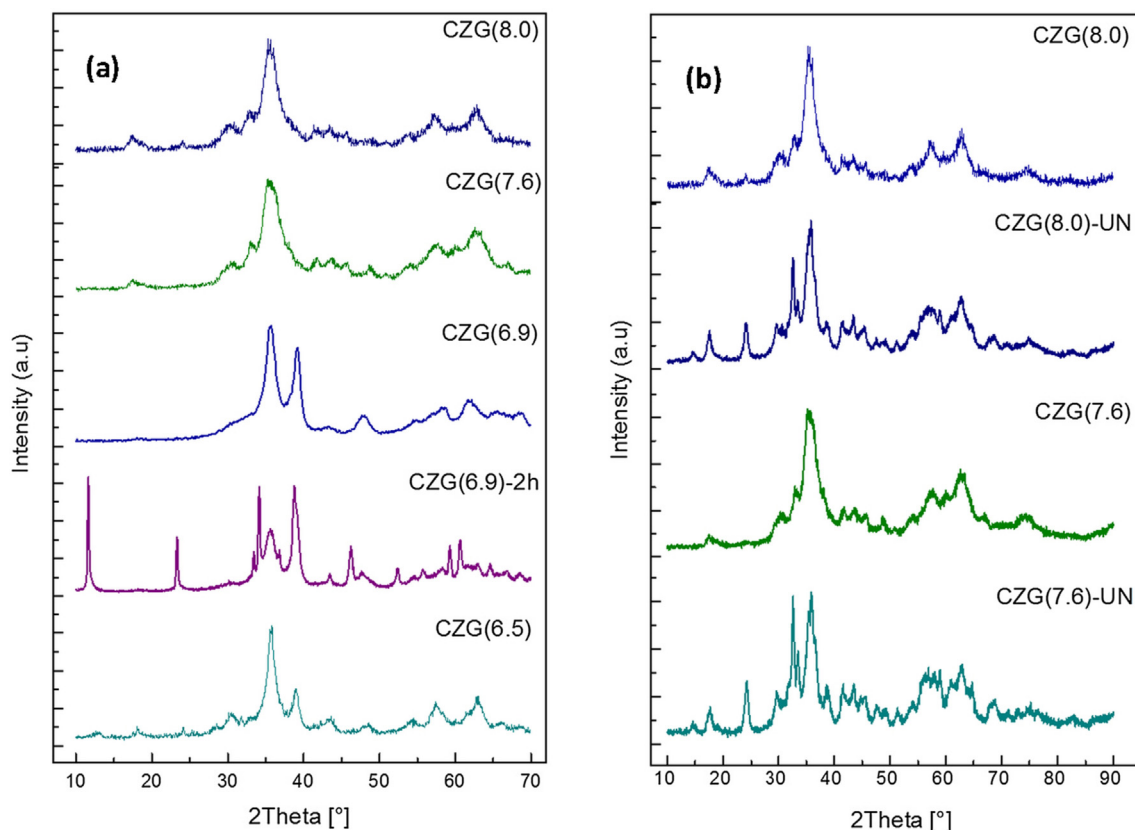


Fig. 2 (a) XRD patterns of co-precipitated CuZnGaO_x catalysts prepared at various pH conditions; (b) XRD patterns of uncalcined, CZG(7.6)-UN and CZG(8.0)-UN, and calcined, CZG(7.6) and CZG(8.0), catalysts.

of CuZnGaO_x catalyst Cu²⁺ in an O_h site manifests to the prolongation and weakening, along with the axial plane, of the Cu–O bonds (Jahn–Teller effect), which leads to removal of axial oxygen. It is assumed that substituting Cu²⁺ for Zn²⁺ (d10) remove or decrease instability of the spinel structure, caused by the Jahn–Teller effect and that there is a higher possibility for Ga³⁺ rather enfold Zn²⁺ than Cu²⁺, which leads to a large excess of free Cu²⁺ in the vicinity to the spinel structure (Tong et al., 2013; Yu et al., 2012).

From XRD analysis (Fig. 2(b)) can be indicated that uncalcined catalysts structure CZG differs from the structure after calcination. The main difference for reduction peaks of uncalcined catalysts is in the disappearance of some peaks and in reconstruction in others after calcination. Peaks at 2θ values of 14.3°, 24.1°, 32.5° and 33.4° with a d-spacing of 6.15 Å, 3.71 Å, 2.75 Å and 2.68 Å corresponded to zincian malachite. The first two peaks disappeared after calcination, while the second two are converted in one smaller peak. The decrease of the zincian malachite phase in a structure is displayed with the second two peaks, on the other hand, a disappearance of the first two peaks demonstrates the transformation of this phase. Reduction peaks at around 2θ values of 57.4° and 62.6° of uncalcined catalysts are reconstructed after calcination in peaks at 2θ values of 57.3° and 62.8° with a d-spacing of 1.61 Å and 1.48 Å both implies more defined structure, corresponding to ZnGa₂O₄. From the results of the XRD analysis of the catalysts CZG(7.6) and CZG(8.0) before and after calcination we can determine the importance of calcination for a catalysts structure and catalytic activity.

Furthermore, for the catalyst CZG(6.9)-2h calcination temperature at 300 °C was maintained for only 2 h, while the catalyst CZG(6–9), which was calcined twice, and all the others co-precipitated catalysts, the temperature 300 °C was maintained for 4 h. As presumed calcination time has an important influence on a structure of a catalyst, which is confirmed by the XRD pattern (Fig. 2). From the XRD profiles can be observed more defined structure for catalyst CZG(6–9) when compared to other catalysts. In catalyst CZG(6–9)-2h structure a zincian malachite (CuZn)CO₃(OH)₂ phase is still present, corresponding to peaks at 2θ values of 11.6° and 23.3° with a d-spacing of 7.66 Å and 3.83 Å (JCPDS 75-1163 or JCPDS 41-1390) (Zhang et al., 2015; Jung et al., 2010). Therefore calcination time and temperature have an important role in catalyst structure. Results attributed that catalyst prepared under low pH environment, i.e. 6.5, produced a larger crystallite size compared with a catalyst synthesised at higher pH conditions. Uncalcined catalysts compared to calcined catalysts prepared at pH values 7.6 and 8.0 indicate the higher crystalline site for uncalcined catalysts, CZG(7.6)-UN and CZG(8.0)-UN (Table 1). Lower crystallinity was obtained for the calcined catalyst CZG(7.6), in comparison with uncalcined catalyst CZG(7.6)-UN; the same applies for catalysts CZG(8.0)-UN and CZG(8.0). The difference in crystallinity indicates different catalyst structure before and after calcination, where the structure of catalysts CZG(7.6)-UN and CZG(8.0)-UN is less amorphous than a structure of calcined catalysts (Electronic supplementary information Table S2). The highest value of crystalline size, calculated from the Scherrer plot (Electronic

supplementary information Figs. S3–S7), for calcined catalyst corresponds to CZG(6.5) (8.1 nm), while the lowest corresponds to the catalyst CZG(8.0) (3.1 nm). This can be attributed to the difference in pH value of preparation, where for higher pH value lower crystalline size is obtained. Furthermore, crystalline size for uncalcined catalyst CZG(8.0)-UN is for 23.9 nm higher compared to calcined catalyst CZG(8.0), this confirms calcination effect on catalyst structure; calcination corresponds to lower crystalline size. The highest value for lattice strain (ϵ), obtained from the slope from the W-H method (Electronic supplementary information Figs. S8–S12), correspond to calcined catalyst CZG(6.9) and uncalcined catalyst CZG(7.6)-UN, 0.12. Lower lattice strain (ϵ) corresponds to catalyst CZG(6.5), 0.03. The UDM (uniform deformation model) attributes the form of W-H method for calculation of crystallite size and strain. The lowest crystalline size calculated from the intercept plotted by W-H method corresponds to calcined catalyst CZG(8.0), 19 nm, while the highest corresponds to uncalcined catalysts CZG(7.6)-UN and CZG(8.0)-UN, 62 nm (Electronic supplementary information Table S2). This might be associated with higher Cu composition in a catalyst which consequently might increase a strain along to a crystalline size.

In H_2 -TPR profiles the main reduction peak is obtained in the range of temperature of 180–260 °C (Fig. 3) for all co-precipitated $CuZnGaO_x$ catalysts, constituted to the CuO reduction. The broader peak could be attributed to electronic interaction with $ZnGaO_x$ (Cai et al., 2015). A shoulder to the main peak is observed for catalyst CZG(6.9) at temperature 143 °C, indicated weakly interacted CuO species. In this work, neither Ga_2O_3 nor ZnO phase was reduced for any of co-precipitated catalysts, due to the selected temperature range for H_2 -TPR analysis, which was too low to reduce any of these phases. This is confirmed by previous studies on that type of catalysts, where a small reduction peak was observed at ~550 °C occurring to the $ZnGaO_x$ spinel phase and no reduction peaks for Ga_2O_3 and ZnO phases (Cai et al., 2015; Tong et al., 2013). Furthermore, catalysts CZG(6.9)-2h and CZG(6.9) have small shoulder before the main reduced peak, which corresponds to weakly reduced CuO . H_2 -TPR results indicate that the catalyst CZG(6.9) has the strongest interaction between CuO and $ZnGaO_x$ considering of its high reduction temperature, 254 °C, while the catalyst CZG(7.6) has the lowest reduction temperature, 203 °C (Table 2), which may have a weak interaction between Cu and Ga . In the recent research (Li et al., 2016) of Cu - Zn catalysts with different composition were shown that the lower temperature reduction of CuO , obtained with H_2 -TPR analysis, occurred for a catalyst with composition from 0.5 to 20 atomic % of Ga^{3+} . The study was shown that the incorporation Ga^{3+} into a catalyst structure, at a lower temperature, stimulate the reduction of some active Cu^{2+} , which corresponded to a lower reduction peak of CuO . It is predicted that Ga^{3+} favour formation of spinel oxide through a hydroxalcite precursor before calcination (Yu et al., 2012). When trivalent Ga^{3+} is added to M^{2+} (Cu^{2+}/Zn^{2+}) in the synthesis of a catalyst the M^{2+} is interlocked in a stable lattice which forms a spinel structure after calcination. The Ga^{3+} has an important role in a structure: it improves a surface area of copper and a decrease in the size of copper, which consequently suppresses the formation of CO (Tong et al., 2013).

Calcination time influence on a catalyst structure can be evidenced by comparing H_2 -TPR analysis of the catalysts

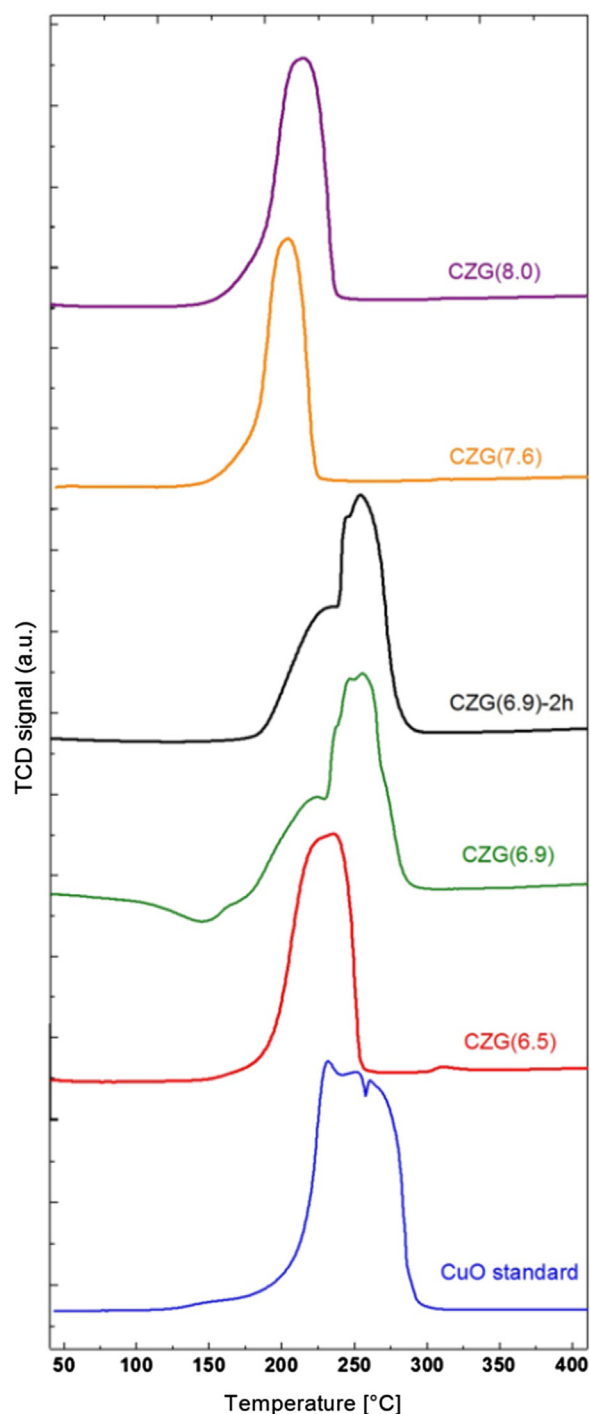


Fig. 3 H_2 -TPR profiles of CuO standard and $CuZnGaO_x$ catalysts prepared at various pH conditions.

CZG(6.9)-2h and CZG(6.9) with other co-precipitated catalysts (Fig. 3). Catalysts CZG(6.9)-2h and CZG(6.9) have three reduction peaks, while other calcined catalysts have one or in one case two (CZG(6.5)) reduction peaks. An amorphous peak starting from 180 °C propose the presence of hydroxyl groups in a catalyst structure, which is supported by XRD. In the study (Smoláková et al., 2015) of Ni/Al_2O_3 and $Ni-Ce/Al_2O_3$ catalysts was indicated that with an increase in calcination temperature of materials reduction temperature of a maximum of a reduction peak, obtained with H_2 -TPR, also increase.

Table 2 H₂-TPR for all CuZnGa co-precipitated catalysts.

| Catalyst | T _{MAX} [°C] ^a | The degree of reduction [%] ^b | H ₂ consumption [10 ⁻³ mmol/g] |
|--------------|---------------------------------------|---|---|
| CZG(6.5) | 235 | 1.9 | 3.9 |
| CZG(6.9)-2h | 231 | 1.9 | 4.0 |
| | 250 | | |
| | 254 | | |
| CZG(6.9) | 224 | 1.5 | 3.2 |
| | 247 | | |
| | 255 | | |
| CZG(7.6) | 203 | 1.3 | 2.6 |
| CZG(8.0) | 214 | 1.9 | 3.9 |
| CuO standard | 229 | 7.2 | |
| | 249 | | 1.5 |
| | 259 | | |

^a In TPR profile.
^b First H₂-TPR analysis.

Tsang (2013) have shown that the spinel structure which includes a surplus of Cu can arrange that Cu as interstitial Cu⁺ in their lattice. The formation of interstitial Cu⁺ propound the significant loss of oxygen at higher temperatures as calcination and this can be described as CuGa₂O₄ ↔ Cu_{1-2x}(Cu_i⁺)_{2x}Ga₂O_{4-x} + 0.5xO₂. That surplus of Cu²⁺ from CuO can form a non-stoichiometric phase by occupying the free lattice site. Their TPR analysis has revealed three individual environments with various degree of Cu reduction in CuZnGaO_x oxide materials. It was suggested that if Cu⁺ occurs close or on the surface of the catalyst, then that is confirmed by αCu reduction site at low temperature, while βCu proves the existence of Cu²⁺ ions inside the cubic non-stoichiometric spinel phase and γCu of Cu²⁺ ions in the tetragonal non-stoichiometric spinel phase. It can be anticipated that all prepared catalysts in this study contain two Cu environments present in the CuZnGaO_x catalyst (αCu and βCu), where αCu peak indicate the reduction of interstitial Cu⁺ species, while βCu peaks are results of reduction of Cu²⁺ from CuO and a mixed oxide matrix.

In catalysts CZG(6.5), CZG(7.6) and CZG(8.0) two Cu environments are present, αCu and βCu. The most narrow reduction peak corresponds to catalyst CZG(7.6), which can be attributed to the prevailing of one Cu environment. Only one environment present in a catalyst structure indicates the possibility that only one catalytic reaction will prevail. The degree of reduction calculated with equations described by Van Der Grift et al. (1991) has the highest value for catalysts CZG(6.9)-2h, CZG(6.5) and CZG(8.0), and the lowest value for catalyst CZG(7.6) (Table 2). H₂ consumption has the highest value for catalysts CZG(6.5) and CZG(8.0), 3.9 10⁻⁶ mol/g (Fig. 4 and Table 2). Catalyst CZG(6.9) shows the highest D_{Cu} and S_{Cu}, 74% and 502 m²_{Cu}/g_{Cu}, while the lowest values correspond to catalyst CZG(6.5) and CZG(8.0), 27% and 185 m²_{Cu}/g_{Cu} (Electronic supplementary information Table S2). With the increase in pH value of catalyst preparation reduction temperature increase, obtained with H₂-TPR, and malachite phase decrease, obtained with XRD. It may be noticed a decrease in Cu dispersion and surface area of Cu with an increase in the pH up to 7.6, and a further increase in the pH i.e. 8.0 decreases the dispersion of copper. This could be related to the amount of

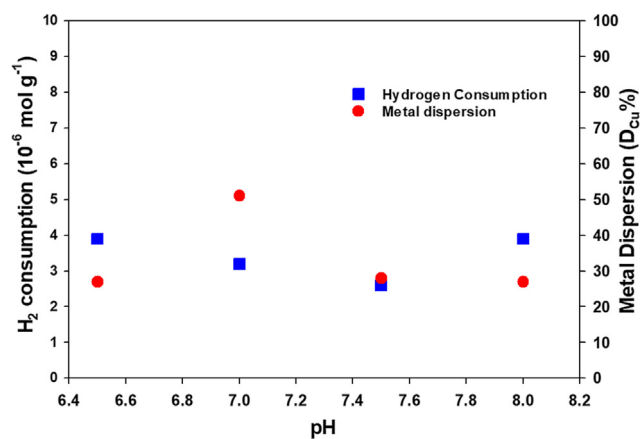


Fig. 4 H₂ consumption (circles) and metal dispersion D_{Cu} (squares) correlation with pH for CuZnGaO_x catalysts.

copper present in the catalyst and to the formation of zinc malachite phases, which is a trend with the hydrogen consumed during TPR. Calcined catalysts CZG(6.5), CZG(6.9)-2h and CZG(8.0) correspond to the highest degree of reduction, 1.9%, while catalyst CZG(7.6) has the lowest value, 1.3%.

From the temperature-programmed desorption profiles of H₂, CO and CO₂ we can observe that H₂ and CO₂ adsorption are higher compared to CO adsorption of the CuZnGaO_x catalysts. H₂ adsorbs molecularly on the reduced copper, CO adsorbs in the form of linear or bridged, and CO₂ adsorbed in the form of monodentate or bidentate carbonates (Yanagisawa and Kashima, 2000; Dong et al., 2003). The results in Table 3 indicate that H₂ and CO₂ adsorption occupies or displaces adsorbed CO from the sites to another type of site. In general, H₂ and CO adsorb on the reduced copper ions (Dong et al., 2003; Rase, 2000). Furthermore, the desorbed ratio of CO molecules to the estimated number of copper active sites was equal to 0.6 i.e. CO adsorbed occupies more than 1/2 of the exposed sites of copper. This would allow the displacement and adsorption of hydrogen to other copper sites. It would lead to a higher concentration of stationary state of active hydrogen species on a surface of the CuZnGaO_x catalyst, particularly at the active interfacial sites of Cu/Zn and Cu/Ga. The H₂/CO and CO₂/CO ratios are higher for the catalyst prepared at a pH of 7.6 which is an indication of a high catalytic behaviour in WGS reaction. Find some references

Temperature Programmed Surface Reaction (TPSR–MS) reaction measurements were conducted over the calcined catalysts, before catalytic testing. Results obtained with TPSR–MS indicate that for the catalyst CZG(8.0) the 100% CO conversion was reached at 260 °C, while for all others catalyst a CO conversion was the same as the temperatures 260 °C and 300 °C, but did not reach 100%. Moles of CO₂ and H₂ produced from WGS for temperatures between 100 °C and 240 °C for the different steam to CO ratios (1: 1 and 1.3: 1) calculated (GASEQ) for equilibrium are represented in supplementary (Electronic supplementary information, Table 1). Equilibrium of CO conversion shows that with an increase of the quantity of steam in the reaction feed the equilibrium conversion also increases. The increase in temperature is in correlation with a decrease in equilibrium CO conversion. At the temperature of 180 °C the catalyst CZG(8.0) indicates the

Table 3 Temperature programmed desorption data (H₂, CO₂, and CO) of CuZnGaO_x co-precipitated catalysts.

| Catalyst | H ₂ desorbed [10 ⁻⁶ mol/g] | CO ₂ desorbed [10 ⁻⁶ mol/g] | CO desorbed [10 ⁻⁶ mol/g] | H ₂ /CO | CO ₂ /CO | Activation Energy (E _a) (KJ mol ⁻¹) |
|-------------|---|--|---|--------------------|---------------------|--|
| CZG(6.5) | 2.8 | 5.1 | 1.2 | 2.33 | 4.25 | 40.1 |
| CZG(6.9)-2h | 3.5 | 5.8 | 1.6 | 2.18 | 3.62 | 45.3 |
| CZG(6.9) | 2.5 | 4.5 | 0.8 | 3.12 | 5.62 | 49.9 |
| CZG(7.6) | 2.4 | 3.5 | 0.5 | 4.80 | 7.00 | 39.2 |
| CZG(8.0) | 3.2 | 5.3 | 1.5 | 2.13 | 3.53 | 35.6 |

highest values for CO (62.5%) and H₂ selectivity (48.9%), while the catalyst CZG(6.5) shows the lowest (57.0% CO and 47.1% H₂ selectivity). The highest value (72.2%) of CO selectivity at the temperature 200 °C corresponds to the catalyst CZG(8.0) and the lowest (65.4%) to the catalyst CZG(6.5) (Fig. 5).

3.1. Results and discussion of catalytic measurements

Measurements of 1 g of each catalyst in a packed bed tubular reactor were made at different temperatures, different flow rates of distilled H₂O and CO (dependent on the H₂O/CO ratios), CO conversion was calculated.

3.1.1. Effect of temperature

Measurements made at different temperatures at a flow rate of distilled water at 0.01 mL/min and STCO value at 1.0 are presented in Fig. 6, which shows the temperature dependence of WGS activity over the catalysts prepared at different pH conditions. In general, the conversion of CO increased with an increase in the temperature from 180 °C to 240 °C. All CO conversions reported in this study are below the equilibrium conversion (Electronic supplementary information, Table 1). At 180 °C with STCO ratio value at 1.0, the highest CO conversion corresponds to the co-precipitated catalysts CZG(8.0), 88.0%, and the following catalysts CZG(6.5), 70.9%, while for the catalyst CZG(6.9) it was the lowest, 37.8%. At the highest temperature at 240 °C for the catalyst prepared at pH value at 8.0 conversion of CO almost reached 100%. Obtained mea-

surements show a correlation between constant pH value of co-precipitated catalyst and CO conversion, an increase in pH value from 6.9 to 8.0 corresponds to an increase in CO conversion. The highest CO conversion of the catalyst CZG(8.0) is in conjunction with its surface area, which is also the highest, 124 m²/g, of among of calcined catalysts.

The apparent activation energy (E_a) for the water gas shift reaction over Cu/Zn/Ga catalysts was determined through the Arrhenius equation in the temperature range of 180–240 °C (Electronic supplementary information, Fig. S13). The activation energy depends on the pH of the preparation, as shown in Table 3. Among all the catalysts, CZG(8.0) catalyst showed lower activation energy of 35.6 KJ mol⁻¹ and CZG(6.9) catalyst showed higher activation energy of 49.9 KJ mol⁻¹ which is in an inverse relationship with the metal dispersion of the catalyst and in agreement with the surface area trend (Table 1).

3.1.2. Effect of water ratio

Higher STCO ratios are used to eliminate undesired reactions (formation of CH₄ or CO disproportionation) which can influence the selectivity of H₂ and CO₂, which will lead to deactivation of the catalyst by carbon deposition (Choung et al., 2005; Reddy et al., 2012). The higher concentration of steam in the feed flow thermodynamically prefers higher CO conversion due to higher catalytic activity, this was reported in some previous studies (Reddy et al., 2012; Shekhar et al., 2012). The surplus of steam has (1) advantageous in increases in the equilibrium conversion (Chen et al., 2008), and (2) disadvantageous in the formation of coke on the catalyst surface

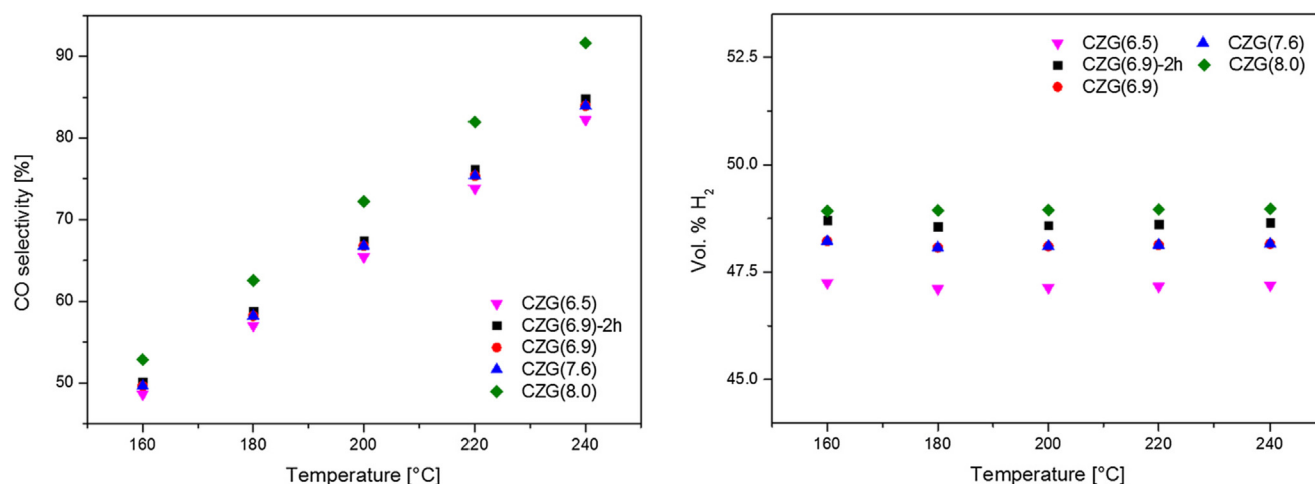


Fig. 5 CO selectivity (left) and vol% of H₂ present (in the outlet gas) in TPSR–MS pattern of WGS reaction over CuZnGaO_x catalysts prepared at various pH values (GHSV = 2200 h⁻¹, STCO ratio of 1.0).

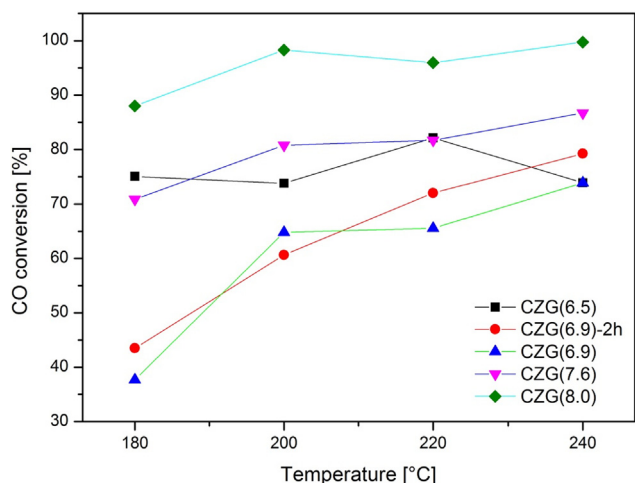


Fig. 6 CO conversion of all synthesised catalysts in temperature dependence, at the flow rate of distilled water 0.01 mL/min and STCO ratio value of 1.0, (GHSV = 1280 h⁻¹).

(Ratnasamy and Wagner, 2009). Reddy et al. (2012) investigated long-term time, 30 days, on the steam stability of Fe/Ce/Cr and Fe/Ce catalysts in high-temperature WGS reaction. They observed that catalyst Fe/Ce at for STCO ratio at 1.5 deactivated with time, because of continuous formation of methane and carbon, while for STCO ratio at 3.5 excellent catalytic stability for WGS reaction was observed. Low STCO ratio, 1.5, showed sooner deactivation; this was in coloration with a quick increase of magnetite in the crystallite size observed in the Fe/Ce catalyst after WGS reaction at an STCO ratio of 1.5 compared to the used catalyst at STCO ratio of 3.5.

A study (Figueiredo et al., 2005) of CO conversion on Cu/ZnO/Al₂O₃ catalysts showed that CO conversion increase continuously with increasing STCO ratio until the constant value was reached. Maroño et al. (2009) have shown that excess of steam in feed flow enhances maximum CO conversion, which provides higher H₂ and lowers CO at higher STCO ratios in the temperature between 250 and 380 °C for the WGS reaction of Fe–Cr based catalysts. Research on Au/CeO₂ by Luengnaruemitchai et al. (2003) revealed that a higher steam concentration (20%) in the feed flow the conversion rapidly increased from 18% to 85% in a temperature range of 200–360 °C. Santos et al. (2017) have shown that in general, the CO conversion increases with increasing the temperature until reaching the equilibrium conversion at which the catalyst performs the maximum conversion due to the thermodynamics. Their research on gold promoted CuO/ZnO/Al₂O₃ catalysts revealed that more than 80% of CO conversion was reached at low temperature (160 °C) and equilibrium conversion was reached at 180 °C for all gold promoted catalysts with different CuO % (w/w) composition (35.74, 41.03 and 43.57%). On the other hand, CO conversion for two uncalcined and not promoted with gold CuO/ZnO/Al₂O₃ catalysts (with a CuO % composition 47%) was reached at 280 °C.

In a recent study (Reina et al., 2016) on gold-based catalysts on WGS performance at 180 °C, the highest CO conversion (68.2%), with a feed flow of 4.5% CO + 30% H₂O balanced in an inert gas, was obtained for the catalyst Au/Ce₂-Cu/Al. Mentioned observations are in an agreement with catalytic results obtained in this study. Measurements for all

prepared catalysts at different STCO ratios and temperatures have shown that higher CO conversion is obtained at higher STCO ratios and higher temperatures. The highest CO conversion was obtained for calcined catalysts CZG(6.5) and CZG(8.0), 99.2% and 98.6%, at temperature 200 °C and the highest STCO ratio, 2. For measurements at STCO 1.3 and flow rate of water 0.01 mL/min at temperature 180 °C the highest CO conversion, 89.3%, correspond to CZG(6.5) following CZG(7.6), 86.9%, while the lowest value corresponds to CZG(6.9)-2h, 39.9%. At the same STCO ratio and temperature, but with flow rate of water at 0.015 mL/min, the highest CO conversion corresponds to catalysts CZG(7.6), 84.6%, and CZG(6.5), 84.4%, while the lowest corresponding to catalyst CZG(6.9)-2h, 36.6% (Figs. 7 and 8).

Furthermore, the WGS reaction is a reversible exothermic reaction; meaning that equilibrium constant and equilibrium CO conversion decrease with increasing temperature and therefore, a CO conversion and production of H₂ are thermodynamically favoured at lower temperatures with a higher quantity of steam, which is supported by results in this study.

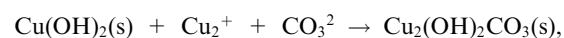
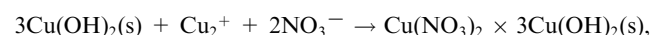
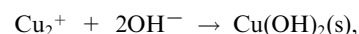
3.1.3. Effect of GHSV

With the increase of GHSV values, the dependent intrinsic activity increases. At temperature 180 °C and STCO ratio 1.3 the highest intrinsic activity, 0.05 mol_{Cu}/g_{catalyst}, at highest GHSV value, 2194 h⁻¹, correspond to calcined catalyst CZG(8.0), following catalyst CZG(7.6), 0.03 mol_{Cu}/g_{catalyst}, while the lowest value corresponds to catalyst CZG(6.9), 0.02 mol_{Cu}/g_{catalyst}. Calcined catalysts CZG(7.6) and CZG(6.5) have the highest intrinsic activity, 0.03 mol_{Cu}/g_{catalyst}, at the highest GHSV, 1926 h⁻¹ at STCO ratio 1.0 (Fig. 9).

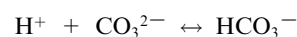
3.1.4. Effect of pH

The highest WGS activity consistent with the value of pH, CO conversion and the metal dispersion can be observed from the catalytic measurements and N₂O chemisorption results (Fig. 10). Sengupta et al. (1989) in their research of Cu–Zn oxide catalysts have shown that the results of reduction and calcination in the formation of a three-component system: metallic copper, zinc oxide and Cu⁺ ions dissolved in zinc oxide. They have shown that the WGS reaction mostly took place by alternate oxidation-reduction of metallic Cu and to a smaller increase on Cu⁺O²⁻ sites in a matrix of zinc oxide.

Important influence of pH on a composition of phase in a precipitates has been reported by many researches. Vasserman (1980) and Li and Inui (1996) proposed the model of reaction for explanation of pH effect in the precipitation:



The decrease in pH value is in coloration with an increase of H⁺ ions. For this reason, the equilibrium shift to the right site and a decrease in carbonate concentration follow:



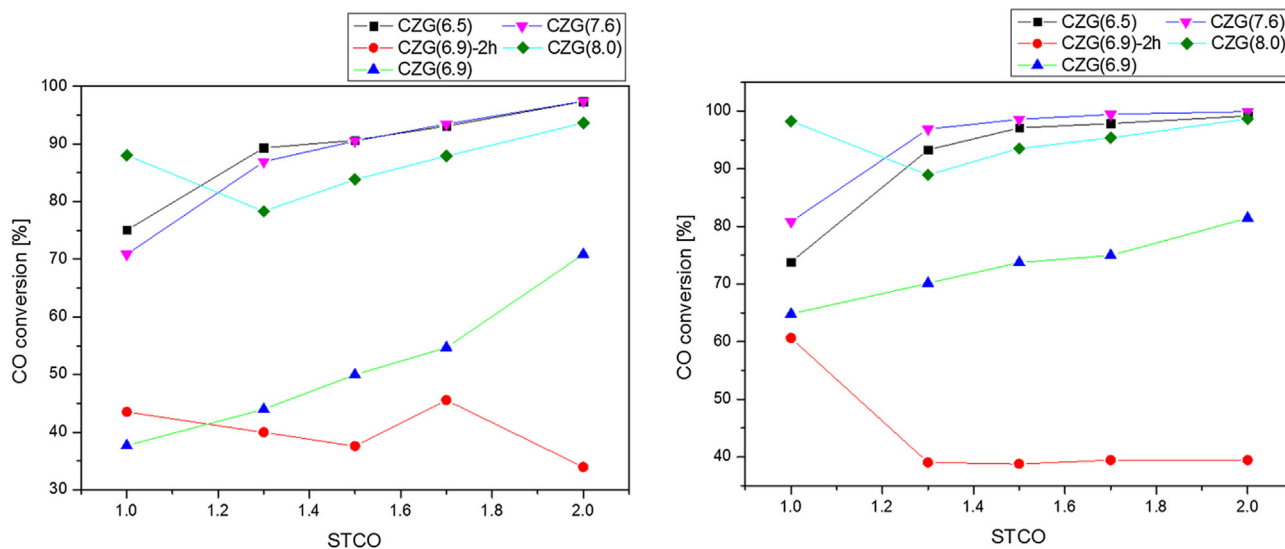


Fig. 7 CO conversion for co-precipitated catalysts CZG(6.5), CZG(6.9)-2h, CZG(6.9), CZG(7.6) and CZG(8.0) at temperatures 180 °C (left) and 200 °C (right) for different STCO ratios (1.0, 1.3, 1.5, 1.7 and 2.0). The flow rate of distillate water corresponds to 0.01 mL/min and GHSV to 1280 h⁻¹.

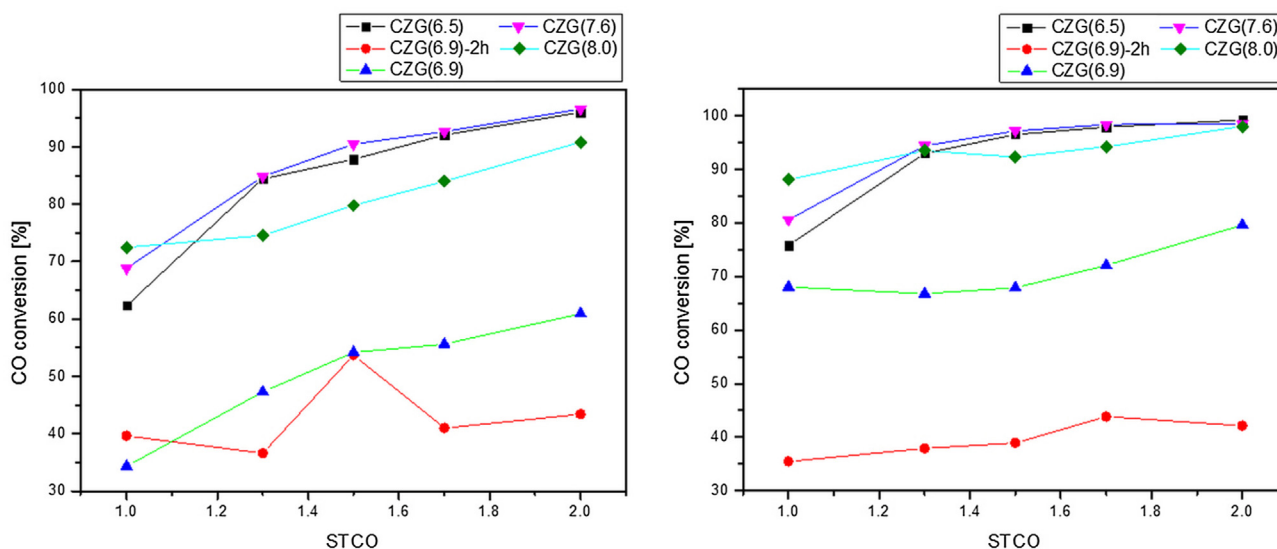


Fig. 8 CO conversion of co-precipitated catalysts CZG(6.5), CZG(6.9)-2h, CZG(6.9), CZG(7.6) and CZG(8.0) at temperatures 180 °C (left) and 200 °C (right) for different STCO ratios (1, 1.3, 1.5, 1.7 and 2.0). The flow rate of distilled water corresponds to 0.015 mL/min and GHSV to 1926 h⁻¹.

This leads to the suppression of the formation of malachite and nitrate phases and other hydroxy carbonates. Li and Inui (1996) and Baltes et al. (2008) proposed that with an increase in pH concentration HCO_3^{2-} and OH^- ions increases, while H^+ ions decrease, which promote a malachite formation and other hydroxy carbonates which lead to increase in $\text{Cu}(\text{OH})_2$ phase formation in a catalyst.

Li et al. (2016) co-precipitated several of Zn–Cu catalysts with a different composition. Their prepared catalysts through the incorporation of Ga^{3+} into the precursor containing Cu and Zn with control of pH value and temperature gave rise to CuZn nanoclusters. In that system ZnGa_2O_4 phase was

clearly created, depended on composition and calcination temperature (> 330 °C). The co-existence of phases ZnGa_2O_4 and ZnO , obtained with XRD, suggested a material interface formation between these two phases. Furthermore, the co-precipitated catalyst at pH 7.6 showed the highest CO conversion (97%) at temperature 200 °C (STCO = 1.3 and water flow rate 0.01 mL/min) compared to prepared catalysts by different methods in literature (Table 4).

The research on Cu/Zn based catalysts with different support (alumina, ceria and silica) prepared by a impregnation method showed, that better catalytic activity was reinforced by high stability and tolerance to start/stop situations, which

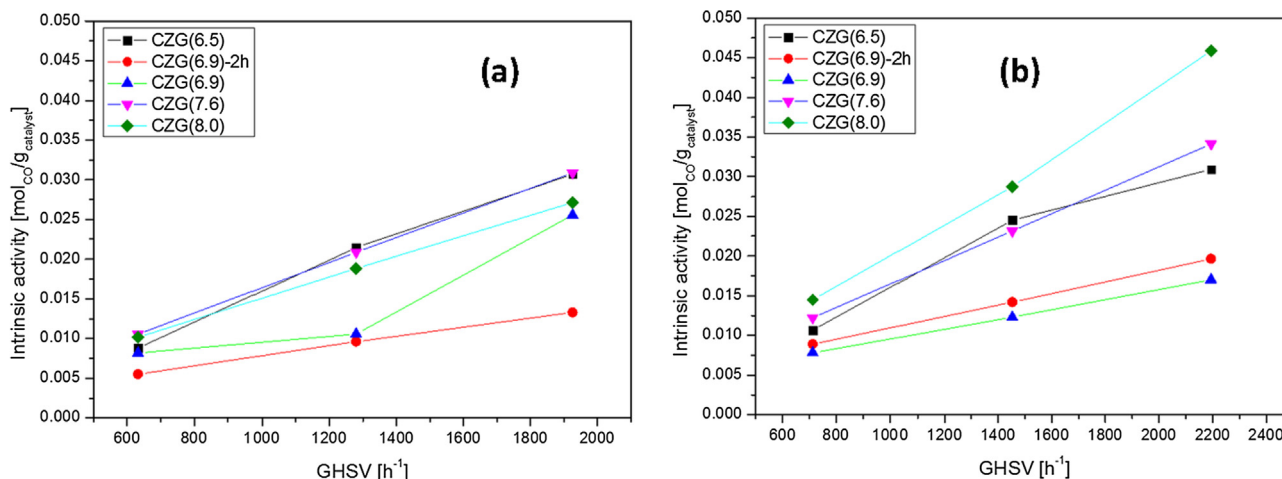


Fig. 9 Intrinsic activity dependence of different GHSV values for precipitated catalysts, at temperature 180 °C and (a) STCO ratio at 1.0 and (b) STCO ratio at value 1.3.

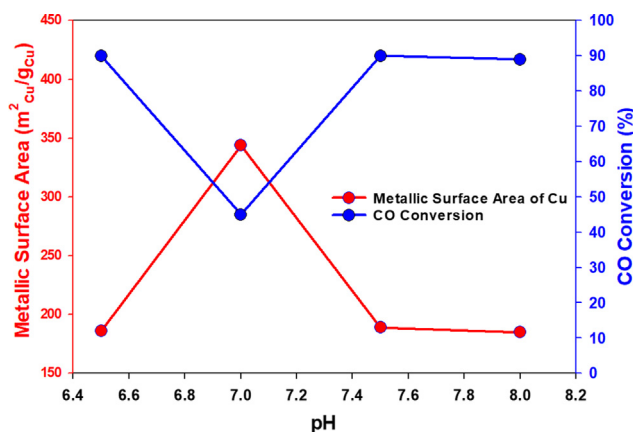


Fig. 10 CO conversion and metallic surface area of Cu correlation with pH for calcined catalysts, at temperature 180 °C, the water flow rate at 0.01 mL/min and STCO ratio at value 1.3.

can be associated to the presence of Ce, which corresponded to decrease in Cu oxidation and sintering (Price et al., 2017). Water-gas shift rates of Cu/ZnO/Cr₂O₃ and Cu/ZnO/Al₂O₃ catalysts in study (Li et al., 2015) of different Cu based catalysts synthesized by the calcination and reduction of Cu-containing layered double hydroxides (LDHs) was higher (75% CO conversion) for the first one, due to high Cu⁰ surface area and interaction among metallic Cu and ZnO on Cu/ZnO/Al₂O₃. Highest CO conversion at temperature 200 °C in the research (Kim et al., 2012) on the co-precipitated Cu–Cr₂O₃–Ga₂O₃ catalysts correspond to the catalyst CuCrGa (1) (Cu/Cr/Ga = 1/0.05/0.05) and it was attributed to the highest metallic surface area (43.6 m²/g) of Cu crystallites. The highest CO conversion (72% at 200 °C) of Cu–Ce–Zn (Tabakova et al., 2007) catalyst prepared by urea-nitrate combustion method was achieved with an increase in surface area and a decrease of Ce particle size and a high WGS rate was achieved by Cu–ZnO/CeAl catalyst prepared by the wet impregnation method. Co-precipitated Cu–Zn–Al-3 (Cu/Zn/Al = 44/44/12) in the study (Fu et al., 2011) of Cu/ZnO/

Al₂O₃ catalysts (Cu/Zn = 1 and Al = 4–24 mol %) with different content of Al, showed the highest CO conversion (95%) with a WGS rate of $15.8 \times 10^{-4} \text{ s}^{-1}$ at temperature 200 °C. High activity was attributed to the structure of the catalyst for which was suggested partially intercalation of aurichalcite into the hydrotalcite and enhanced the interaction among the supports and active centers of the catalyst.

4. Conclusions

The present study demonstrates the importance of catalyst preparation, where its structure is strongly dependent on pH value at which catalysts were co-precipitated, drying and calcination (calcination time), to summarise, all steps of catalyst preparation have an important influence on catalyst structure. Furthermore, from the catalyst structure, catalytic activity, stability, and selectivity are dependent. Selected parameters (STCO ratio, temperature, the flow rate of water), at which measurements for WGS reaction took place, have an important influence on CO conversion. Therefore, it is extremely significant to synthesise catalysts at the right constant pH value and to choose parameters, which provide the highest catalytic activity for the WGS reaction. The surface areas for co-precipitated catalysts CuZnGaO_x ranged between 55–125 m²/g, where the highest surface area, 124 m²/g, was obtained for the catalysts prepared at higher pH values, i.e. 7.6 and 8.0.

Powder XRD analysis indicates a difference in catalytic structure comparing uncalcined to calcined catalysts CuZnGaO_x, determined the importance of calcination for catalyst structure and subsequently catalytic activity. With an increase in pH value of catalyst preparation reduction temperature increase, obtained with H₂-TPR, and malachite phase decrease, obtained with XRD. Catalytic measurements obtained at temperature 180 °C with STCO ratio value at 1.0 shows a correlation between the Cu metallic surface area and CO conversion; an increase in Cu metallic surface area the CO conversion. Experiments at different STCO ratios and temperatures for all calcinated catalysts have shown higher CO conversion at higher STCO ratios and higher temperatures. With the increase of GHSV values, an intrinsic activity also increases. At temperature 180 °C and STCO ratio

Table 4 Comparison of activity of CuZnGaO_x catalyst with the other catalysts reported in the literature.

| Catalyst | Preparation method | GHSV (h ⁻¹) | WGS rate* | Reference |
|--|-------------------------|-------------------------|-----------|-------------------------|
| Cu-ZnO/ZSM-5 | wet impregnation | 9000 | 3.5 | (Price et al., 2017) |
| Cu-ZnO/Si | wet impregnation | 9000 | 10.9 | (Price et al., 2017) |
| Cu-ZnO/Al commercial | co-precipitation | 4000 | 0.8 | (Price et al., 2017) |
| Cu/ZnO/Al ₂ O ₃ commercial | co-precipitation | 8000 | 1.1 | (Li et al., 2015) |
| CuCrGa(1) | co-precipitation | 4000 | 1.0 | (Kim et al., 2012) |
| Cu/ZnO/Cr ₂ O ₃ | co-precipitation | 8000 | 1.3 | (Li et al., 2015) |
| Cu-Ce-Zn | urea-nitrate combustion | 4000 | 1.1 | (Tabakova et al., 2007) |
| Cu/ZnO/Al ₂ O ₃ | co-precipitation | 8000 | 1.4 | (Li et al., 2015) |
| Cu/ZnO/Al ₂ O ₃ | wet impregnation | 9000 | 20.4 | (Price et al., 2017) |
| Cu-Zn-Al4 | co-precipitation | 6000 | 13.4 | (Fu et al., 2011) |
| Cu-ZnO/CeAl | wet impregnation | 9000 | 10.3 | (Price et al., 2017) |
| Cu-Zn-Al | co-precipitation | 6000 | 15.8 | (Fu et al., 2011) |
| CZG(7.6) | co-precipitation | 2200 | 21.8 | This work |

* (mol of CO converted/s × mol active phase × 10⁴).

1.0 the highest intrinsic activity, 0.05 mol_{Cu}/g_{catalyst}, at the highest GHSV value, 2194 h⁻¹, corresponds to calcined catalyst CZG(8.0). At temperature 200 °C the co-precipitated catalyst at pH value 7.6 showed the highest CO conversion, 97%, compared with prepared catalysts by different methods and commercial catalysts in the literature.

Declaration of Competing Interest

The authors declare that they have no known competing financial interests or personal relationships that could have appeared to influence the work reported in this paper.

Acknowledgments

The research was funded by NATO in the framework of the Science for Peace and Security (SPS) Programme under agreement EAP.SFPP 984738. The provision of financial support for the conduct of the research and preparation of the article by the Slovenian Research Agency (ARRS) (Program P2-0152) is gratefully acknowledged.

Appendix A. Supplementary material

Supplementary data to this article can be found online at <https://doi.org/10.1016/j.arabjc.2020.02.005>.

References

- Aeijselts Averink Silberova, B., Mul, G., Makkee, M., Moulijn, J.A., 2006. DRIFTS study of the water–gas shift reaction over Au/Fe₂O₃. *J. Catal.* 243, 171–182.
- Agrell, J., Hasselbo, K., Jansson, K., Järås, S.G., Boutonnet, M., 2001. Production of hydrogen by partial oxidation of methanol over Cu/ZnO catalysts prepared by microemulsion technique. *Appl. Catal. A*. 211, 239–250.
- Al-Fatesh, A.S.A., Fakeeha, A.H., 2012. Effects of calcination and activation temperature on dry reforming catalysts. *J. Saudi Chem. Soc.* 16, 55–61.
- Baltes, C., Vukojević, S., Schüth, F., 2008. Correlations between synthesis, precursor, and catalyst structure and activity of a large set of CuO/ZnO/Al₂O₃ catalysts for methanol synthesis. *J. Catal.* 258, 334–344.
- Bart, J.C.J., Sneed, R.P.A., 1987. Copper-zinc oxide-alumina methanol catalysts revisited. *Catal. Today*. 2, 1–124.
- Basińska, A., Kępiński, L., Domka, F., 1999. The effect of support on WGS activity of ruthenium catalysts. *Appl. Catal. A*. 183, 143–153.
- Behrens, M., 2009. Meso- and nano-structuring of industrial Cu/ZnO/(Al₂O₃) catalysts. *J. Catal.* 267, 24–29.
- Behrens, M., Schlögl, R., 2013. How to prepare a good Cu/ZnO catalyst or the role of solid state chemistry for the synthesis of nanostructured catalysts. *Zeitschrift für anorganische und allgemeine Chemie* 639, 2683–2695.
- Boudjemaa, A., Auroux, A., Boumaza, S., Trari, M., Cherifi, O., Bouarab, R., 2009. Hydrogen production on iron–magnesium oxide in the high-temperature water-gas shift reaction. *React. Kinet. Catal. Lett.* 98, 319–325.
- Cai, W., de la Piscina, P.R., Toyir, J., Homs, N., 2015. CO₂ hydrogenation to methanol over CuZnGa catalysts prepared using microwave-assisted methods. *Catal. Today*. 242 (Part A), 193–199.
- Carl, Bosch, 1914. Wild Wilhelm. Canadian patent 153 379.
- Chen, W.-H., Hsieh, T.-C., Jiang, T.L., 2008. An experimental study on carbon monoxide conversion and hydrogen generation from water gas shift reaction. *Energy Convers. Manage.* 49, 2801–2808.
- Chenu, E., Jacobs, G., Crawford, A.C., Keogh, R.A., Patterson, P.M., Sparks, D.E., et al., 2005. Water-gas shift: an examination of Pt promoted MgO and tetragonal and monoclinic ZrO₂ by in situ drifts. *Appl. Catal. B*. 59, 45–56.
- Choung, S.Y., Ferrandon, M., Krause, T., 2005. Pt-Re bimetallic supported on CeO₂-ZrO₂ mixed oxides as water–gas shift catalysts. *Catal. Today*. 99, 257–262.
- de Souza Gonçalves, A., Antonio Marques de Lima, S., Rosaly Davolos, M., Gutierrez Antônio, S., de Oliveira Paiva-Santos, C., 2006. The effects of ZnGa₂O₄ formation on structural and optical properties of ZnO:Ga powders. *J. Solid State Chem.* 179, 1330–1334.
- Dong, X., Zhang, H.-B., Lin, G.-D., Yuan, Y.-Z., Tsai, K.R., 2003. Highly active CNT-promoted Cu–ZnO–Al₂O₃ catalyst for methanol synthesis from H₂/CO/CO₂. *Catal. Lett.* 85, 237–246.
- Faungnawakij, K., Tanaka, Y., Shimoda, N., Fukunaga, T., Kikuchi, R., Eguchi, K., 2007. Hydrogen production from dimethyl ether steam reforming over composite catalysts of copper ferrite spinel and alumina. *Appl. Catal. B* 74, 144–151.
- Figueiredo, R.T., Ramos, A.L.D., de Andrade, H.M.C., Fierro, J.L.G., 2005. Effect of low steam/carbon ratio on water gas shift reaction. *Catal. Today*. 107–108, 671–675.
- Fu, W., Bao, Z., Ding, W., Chou, K., Li, Q., 2011. The synergistic effect of the structural precursors of Cu/ZnO/Al₂O₃ catalysts for water–gas shift reaction. *Catal. Commun.* 12, 505–509.

- Gokhale, A.A., Dumesic, J.A., Mavrikakis, M., 2008. On the mechanism of low-temperature water gas shift reaction on copper. *J. Am. Chem. Soc.* 130, 1402–1414.
- Hadden, R.A., Lambert, P.J., Ranson, C., 1995. Relationship between the copper surface area and the activity of CuO/ZnO/Al₂O₃ water-gas shift catalysts. *Appl. Catal. A* 122, L1–L4.
- Hodge, N.A., Kiely, C.J., Whyman, R., Siddiqui, M.R.H., Hutchings, G.J., Pankhurst, Q.A., et al, 2002. Microstructural comparison of calcined and uncalcined gold/iron-oxide catalysts for low-temperature CO oxidation. *Catal. Today* 72, 133–144.
- Jha, A., Jeong, D.-W., Lee, Y.-L., Jang, W.-J., Shim, J.-O., Jeon, K.-W., et al, 2016. Chromium free high temperature water–gas shift catalyst for the production of hydrogen from waste derived synthesis gas. *Appl. Catal. A* 522, 21–31.
- Jung, H., Yang, D.R., Joo, O.S., Jung, K.D., 2010. The importance of the aging time to prepare Cu/ZnO/Al₂O₃ catalyst with high surface area in methanol synthesis. *Bull. Korean Chem. Soc.* 31, 1241–1246.
- Jung, H., Yang, D.-R., Joo, O.-S., Jung, K.-D., 2010. The importance of the aging time to prepare Cu/ZnO/Al₂O₃ catalyst with high surface area in methanol synthesis. *Bull. Korean Chem. Soc.* 31, 1241–1246.
- Khorsand Zak, A., Abd Majid, W.H., Abrishami, M.E., Yousefi, R., 2011. X-ray analysis of ZnO nanoparticles by Williamson-Hall and size–strain plot methods. *Solid State Sci.* 13, 251–256.
- Kim, A.R., Lee, B., Park, M.J., Moon, D.J., Bae, J.W., 2012. Catalytic performance on CuO–Cr₂O₃–Ga₂O₃ mixed oxides for water gas shift reaction: Effects of Ga/Cr molar ratio. *Catal. Commun.* 19, 66–69.
- Li, D., Cai, Y., Ding, Y., Li, R., Lu, M., Jiang, L., 2015. Layered double hydroxides as precursors of Cu catalysts for hydrogen production by water-gas shift reaction. *Int. J. Hydrog. Energy* 40, 10016–10025.
- Li, J.L., Inui, T., 1996. Characterization of precursors of methanol synthesis catalysts, copper/zinc/aluminum oxides, precipitated at different pHs and temperatures. *Appl. Catal. A* 137, 105–117.
- Li, L., Mao, D., Xiao, J., Li, L., Guo, X., Yu, J., 2016. Facile preparation of highly efficient CuO–ZnO–ZrO₂/HZSM-5 bifunctional catalyst for one-step CO₂ hydrogenation to dimethyl ether: Influence of calcination temperature. *Chem. Eng. Res. Des.* 111, 100–108.
- Li, M.M.-J., Zheng, J., Qu, J., Liao, F., Raine, E., Kuo, W.C.H., et al, 2016. The remarkable activity and stability of a highly dispersive beta-brass Cu–Zn catalyst for the production of ethylene glycol. *Sci. Reports* 6, 20527.
- Luengnarumitchai, A., Osuwan, S., Gulari, E., 2003. Comparative studies of low-temperature water–gas shift reaction over Pt/CeO₂, Au/CeO₂, and Au/Fe₂O₃ catalysts. *Catal. Commun.* 4, 215–221.
- Luo, W., Jing, F.-L., Yu, X.-P., Sun, S., Luo, S.-Z., Chu, W., 2012. Synthesis of 2-Methylpyrazine Over Highly Dispersed Copper Catalysts. *Catal. Lett.* 142, 492–500.
- Maroño, M., Ruiz, E., Sánchez, J.M., Martos, C., Dufour, J., Ruiz, A., 2009. Performance of Fe–Cr based WGS catalysts prepared by co-precipitation and oxi-precipitation methods. *Int. J. Hydrog. Energy* 34, 8921–8928.
- Melián-Cabrera, I., López Granados, M., Fierro, J.L.G., 2002. Reverse topotactic transformation of a Cu–Zn–Al catalyst during wet Pd impregnation: relevance for the performance in methanol synthesis from CO₂/H₂ mixtures. *J. Catal.* 210, 273–284.
- Mi, J., Zhang, J., Cao, Y., Chen, C., Lin, X., Chen, J., et al, 2017. Sulfur resistant WGS catalyst for hydrogen production based on CoMo supported by Nb modified MgAl mixed oxide. *Int. J. Hydrog. Energy* 42, 29935–29943.
- Mond, L., 1889. Process of obtaining hydrogen gas. Google Patents.
- Mote, V., Purushotham, Y., Dole, B., 2012. Williamson-Hall analysis in estimation of lattice strain in nanometer-sized ZnO particles. *J. Theor. Appl. Phys.* 6, 1–8.
- Panagiotopoulou, P., Christodoulakis, A., Kondarides, D.I., Boghosian, S., 2006. Particle size effects on the reducibility of titanium dioxide and its relation to the water–gas shift activity of Pt/TiO₂ catalysts. *J. Catal.* 240, 114–125.
- Price, C., Pastor-Pérez, L., le Saché, E., Sepúlveda-Escribano, A., Reina, T.R., 2017. Highly active Cu–ZnO catalysts for the WGS reaction at medium–high space velocities: Effect of the support composition. *Int. J. Hydrog. Energy* 42, 10747–10751.
- Rase, H.F., 2000. Handbook of Commercial Catalysts: Heterogeneous Catalysts. Taylor & Francis.
- Ratnasamy, C., Wagner, J.P., 2009. Water gas shift catalysis. *Catal. Rev.* 51, 325–440.
- Reddy, G.K., Kim, S.J., Dong, J., Smirniotis, P.G., Jasinski, J.B., 2012. Long-term WGS stability of Fe/Ce and Fe/Ce/Cr catalysts at high and low steam to CO ratios—XPS and Mössbauer spectroscopic study. *Appl. Catal. A* 415–416, 101–110.
- Reina, T.R., Ivanova, S., Centeno, M.A., Odriozola, J.A., 2016. The role of Au, Cu & CeO₂ and their interactions for an enhanced WGS performance. *Appl. Catal. B* 187, 98–107.
- Reitz, W., 2007. Handbook of fuel cells: fundamentals, technology, and applications. In: Vielstich, W., Lamm, A., Gasteiger, H.A. (eds.), *Materials and Manufacturing Processes*, vol. 1. 22:788–.
- Rubin, K., Pohar, A., Dasireddy, V.D.B.C., Likozar, B., 2018. Synthesis, characterization and activity of CuZnGaO_x catalysts for the water–gas shift (WGS) reaction for H₂ production and CO removal after reforming. *Fuel Process Technol.* 169, 217–225.
- Santos, J.L., Reina, T.R., Ivanova, S., Centeno, M.A., Odriozola, J. A., 2017. Gold promoted Cu/ZnO/Al₂O₃ catalysts prepared from hydrotalcite precursors: Advanced materials for the WGS reaction. *Appl. Catal. A* 201, 310–317.
- Schüth, F., Unger, K., 2008. Precipitation and Coprecipitation. Preparation of Solid Catalysts. Wiley-VCH Verlag GmbH, pp. 60–84.
- Sengupta, G., Das, D.P., Kundu, M.L., Dutta, S., Roy, S.K., Sahay, R.N., et al, 1989. Study of copper–zinc oxide catalysts, characterisation of the coprecipitate and mixed oxide. *Appl. Catal.* 55, 165–180.
- Shekhar, M., Wang, J., Lee, W.-S., Williams, W.D., Kim, S.M., Stach, E.A., et al, 2012. Size and support effects for the water-gas shift catalysis over gold nanoparticles supported on model Al₂O₃ and TiO₂. *J. Am. Chem. Soc.* 134, 4700–4708.
- Shishido, T., Yamamoto, Y., Morioka, H., Takaki, K., Takehira, K., 2004. Active Cu/ZnO and Cu/ZnO/Al₂O₃ catalysts prepared by homogeneous precipitation method in steam reforming of methanol. *Appl. Catal. A* 263, 249–253.
- Si, R., Raitano, J., Yi, N., Zhang, L., Chan, S.-W., Flytzani-Stephanopoulos, M., 2012. Structure sensitivity of the low-temperature water-gas shift reaction on Cu–CeO₂ catalysts. *Catal. Today* 180, 68–80.
- Smith, R.J.B., Loganathan, M., Shantha, Murthy S., 2010. A review of the water gas shift reaction kinetics. *Int. J. Chem. React. Eng.* 8, 1542–6580.
- Smoláková, L., Kout, M., Koudelková, E., Čapek, L., 2015. Effect of calcination temperature on the structure and catalytic performance of the Ni/Al₂O₃ and Ni–Ce/Al₂O₃ catalysts in oxidative dehydrogenation of ethane. *Ind. Eng. Chem. Res.* 54, 12730–12740.
- Su, D.S., Zhang, B., Schlögl, R., 2015. Electron microscopy of solid catalysts—transforming from a challenge to a toolbox. *Chem. Rev.* 115, 2818–2882.
- Tabakova, T., Idakiev, V., Papavasilou, J., Avgouropoulos, G., Ioannides, T., 2007. Effect of additives on the WGS activity of combustion synthesized CuO/CeO₂ catalysts. *Catal. Commun.* 8, 101–106.
- Thinon, O., Diehl, F., Avenier, P., Schuurman, Y., 2008. Screening of bifunctional water-gas shift catalysts. *Catal. Today* 137, 29–35.
- Tong, W., West, A., Cheung, K., Yu, K.-M., Tsang, S.C.E., 2013. Dramatic effects of gallium promotion on methanol steam

- reforming Cu-ZnO catalyst for hydrogen production: formation of 5 Å copper clusters from Cu-ZnGaOx. *ACS Catal.* 3, 1231–1244.
- Tong, W., Cheung, K., West, A., Yu, K.-M., Tsang, S.C.E., 2013. Direct methanol steam reforming to hydrogen over CuZnGaOx catalysts without CO post-treatment: mechanistic considerations. *Phys. Chem. Chem. Phys.* 15, 7240–7248.
- Toyir, J., Ramírez de la Piscina, P., Homs, N., 2015. Ga-promoted copper-based catalysts highly selective for methanol steam reforming to hydrogen; relation with the hydrogenation of CO₂ to methanol. *Int. J. Hydrog. Energy* 40, 11261–11266.
- Tsang, S.C.E., 2013. Steam reforming of methanol. Google Patents.
- Twigg, M.V., 1996. *Catalyst Handbook*. Manson Pub.
- Van Der Grift, C.J.G., Wielers, A.F.H., Jogh, B.P.J., Van Beunum, J., De Boer, M., Versluijs-Helder, M., et al, 1991. Effect of the reduction treatment on the structure and reactivity of silica-supported copper particles. *J. Catal.* 131, 178–189.
- Vasserman, I., 1980. *Chemical Precipitation from Solutions*. Khimiya, Leningrad.
- Yahiro, H., Murawaki, K., Saiki, K., Yamamoto, T., Yamaura, H., 2007. Study on the supported Cu-based catalysts for the low-temperature water-gas shift reaction. *Catal. Today* 126, 436–440.
- Yanagisawa, Y., Kashima, S-i, 2000. Interaction of CO with CaO surfaces: A TPD and FTIR study. *Surf Sci.* 454, 379–383.
- Yu, K.M.K., Tong, W., West, A., Cheung, K., Li, T., Smith, G., et al, 2012. Non-syngas direct steam reforming of methanol to hydrogen and carbon dioxide at low temperature. *Nat. Commun.* 3, 1230.
- Yuan, Z., Wang, L., Wang, J., Xia, S., Chen, P., Hou, Z., et al, 2011. Hydrogenolysis of glycerol over homogeneously dispersed copper on solid base catalysts. *Appl. Catal. B.* 101, 431–440.
- Zhang, Q.-C., Liu, Z.-W., Zhu, X.-H., Wen, L.-X., Zhu, Q.-F., Guo, K., et al, 2015. Application of microimpinging stream reactors in the preparation of CuO/ZnO/Al₂O₃ catalysts for methanol synthesis. *Ind. Eng. Chem. Res.* 54, 8874–8882.